Journal of Materials Chemistry A



PAPER

View Article Online
View Journal | View Issue



Cite this: *J. Mater. Chem. A*, 2020, **8**, 24563

Understanding activity origin for the oxygen reduction reaction on bi-atom catalysts by DFT studies and machine-learning†

Chaofang Deng, ‡^{ab} Yang Su, (1) ‡^b Fuhua Li, b Weifeng Shen, (1) Zhongfang Chen (1) *c and Qing Tang (1) *b

Bi-atom catalysts (BACs) have attracted increasing attention in important electrocatalytic reactions such as the oxygen reduction reaction (ORR). Here, by means of density functional theory simulations coupled with machine-learning technology, we explored the structure-property correlation and catalytic activity origin of BACs, where metal dimers are coordinated by N-doped graphene (NC). We first sampled 26 homonuclear (M₂/NC) BACs and constructed the activity volcano curve. Disappointingly, only one BAC, namely Co₂/NC, exhibits promising ORR activity, leaving considerable room for enhancement in ORR performance. Then, we extended our study to 55 heteronuclear BACs (M₁M₂/NC) and found that 8 BACs possess competitive or superior ORR activity compared with the Pt(111) benchmark catalyst. Specifically, CoNi/NC shows the most optimal activity with a very high limiting potential of 0.88 V. The linear scaling relationships among the adsorption free energy of *OOH, *O and *OH species are significantly weakened on BACs as compared to a transition metal surface, indicating that it is difficult to precisely describe the catalytic activity with only one descriptor. Thus, we adopted machine-learning techniques to identify the activity origin for the ORR on BACs, which is mainly governed by simple geometric parameters. Our work not only identifies promising BACs yet unexplored in the experiment, but also provides useful guidelines for the development of novel and highly efficient ORR catalysts.

Received 15th August 2020 Accepted 3rd November 2020

DOI: 10.1039/d0ta08004g

rsc.li/materials-a

Introduction

The use of a proton exchange membrane fuel cell (PEMFC) is an attractive approach to produce electrical energy from direct electrochemical conversion of oxygen and hydrogen.^{1,2} However, to make the PEMFC process economically attractive, there are many challenges to be overcome, and one of them is the slow kinetics of the oxygen reduction reaction (ORR) at the cathode.³⁻⁵ The key to improving the sluggish ORR performance is to find a viable and highly active electrocatalyst.⁶⁻¹⁰ Presently, Pt and its alloys remain the most common and efficient electrocatalysts,¹¹⁻¹⁴ yet their drawbacks of scarcity and poor durability give rise to large obstacles on their widespread applications. This

thus calls for the development of more promising and costeffective alternatives to ORR electrocatalysts.

In recent years, single-atom catalysts (SACs), where active metal atoms are singly distributed on a support, have attracted tremendous research attention.15-21 Despite significant advances made in SACs, their capabilities toward the ORR are still unsatisfactory, making it a great challenge to develop new efficient ORR electrocatalysts. Notably, recent experimental and theoretical studies showed that introducing secondary metal atoms can modulate the electronic properties to further boost the activity of SACs, indicating the great prospect of bi-atom catalysts (BACs).²²⁻³⁰ Experimentally, among others, Xiao et al. synthesized binuclear Co2N5 active sites, which showed much higher ORR activity than single CoN₄ active sites.²³ Remarkably, Han et al. demonstrated that binary CoNi sites in nitrogendoped hollow carbon nanocubes exhibit outstanding catalytic performance for bifunctional oxygen reduction and evolution reactions.24 Theoretically, Guo et al. showed that BACs can help overcome the activity and selectivity challenges of catalysts towards electrochemical nitrogen reduction,27 and Li et al. demonstrated that a heteronuclear BAC, Fe₁Cu₁@C₂N, outperformed its homonuclear counterparts (Fe2@C2N and Cu₂@C₂N) towards CO oxidation.²⁸ These studies indicate that not only homo-nuclear but also hetero-nuclear metal dimers can function as potential ORR electrocatalysts,

^aCooperative Innovation Center of Lipid Resources and Children's Daily Chemicals, Chongqing University of Education, Chongqing 400067, China

^bSchool of Chemistry and Chemical Engineering, Chongqing Key Laboratory of Theoretical and Computational Chemistry, Chongqing University, Chongqing 401331, China. E-mail: qingtang@cqu.edu.cn

Department of Chemistry, University of Puerto Rico, Rio Piedras, San Juan, PR 00931, USA. E-mail: zhongfangchen@gmail.com

[†] Electronic supplementary information (ESI) available: Computational details, adsorption free energy, limiting potential, formation energy and the adsorption geometry of ORR intermediates and input features of machine-learning. See DOI: 10.1039/d0ta08004g

[‡] Dr Chaofang Deng and Dr Yang Su contributed equally to this work.

heteronuclear BACs may behave ever better. Despite this recent progress, the development of BACs is still in its infancy. The underlying activity origin and possible structure–activity correlation of BACs still remain unclear. These urgent issues lay the foundation for the rational design of efficient BACs for the ORR. In particular, considering the large number of transition metals in the periodic table, combinatorial possible homo- and heterobi-atom dimers are numerically very high, which makes it a grand experimental challenge to synthesize and characterize all potential combinations. To this end, theoretical calculations aided by data-mining techniques, such as machine-learning, are highly promising to fast screen high-performance catalyst candidates and understand the origin behind the activity of BACs.

Note that traditional SACs can be regarded as the smallest size limit of pure metals, while BACs, hetero-bi-metals, in particular, can be viewed as the size limit of hybrid alloy materials. To accelerate the discovery of prospective BACs, herein, systematic density functional theory (DFT) calculations were employed to explore the ORR activity of BACs. Taking N-doped graphene (NC) as the stabilizing substrate, we explored the ORR activity of metal dimers anchored on NC and sampled the large potential combination space of both homonuclear (M₂/NC) and heteronuclear (M₁M₂/NC) BACs. We demonstrated that one homonuclear BAC and eight heteronuclear BACs can achieve remarkable activity improvement, which is comparable or even superior to that of Pt-based catalysts. Among them, a noble metal-free BAC, namely CoNi/NC, shows the most optimal activity with a very high limiting potential of 0.88 V.

Furthermore, by combining the machine-learning method, we identified the key factor that governs the ORR activity of BACs. The geometric distance between the metal dimer and the coordinated N and the distance between the two metal centers are found to play the key role. This work not only identifies highly promising BACs to replace precious Pt catalysts, but also provides practical guidance for discovering and designing high-performance catalysts.

Methods

Spin-polarized DFT calculations were performed using the Vienna ab initio simulation package (VASP).31 The electron exchange-correlation was represented by the Perdew-Burke-Ernzerhof (PBE) functional with generalized gradient approximation (GGA).32 The interaction between ion cores and valence electrons was described by the projector augmented wave (PAW) method.33 The cutoff energy was set as 400 eV and the Brillouin zone was sampled using $3 \times 3 \times 1$ k-points. A vacuum space of 15 Å was adopted to minimize interactions between neighboring catalyst images. A dispersion correction using the DFT-D3 method was carried out to describe the van der Waals (vdW) interactions between the reactants and the catalyst.34 To simulate the H2O solvent environment, the Poisson-Boltzmann implicit solvation model was employed with a dielectric constant of $\varepsilon = 80$ for water. ^{35,36} The convergence threshold was set to be 1×10^{-5} eV for energy and 0.02 eV Å⁻¹ for atomic force. To correct the magnetization, we considered different initial magnetic moments and smearing values. It was found that the

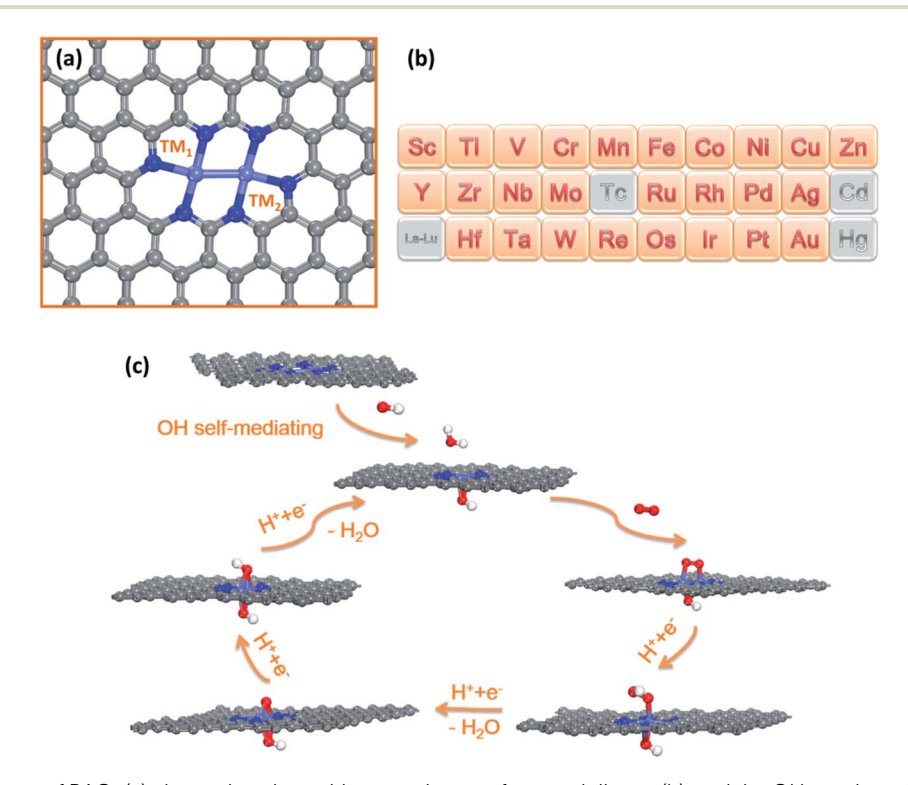


Fig. 1 Geometric structure of BACs (a), the explored transition metal atoms for metal dimers (b), and the OH species self-mediating mechanism on BACs (c).

initial magnetic moment had little influence on the converged magnetic moments. However, the magnetic moments were sensitive to the smearing value. When a smearing width of 0.001 eV was adopted, the magnetic moment of the metal dimer (Fe₂: 3 μ_B , Co₂: 1 μ_B , and Ni₂: 0 μ_B) was close to the results from a previous report.37 Thus, the smearing width was set as 0.001 eV for our DFT calculations. The catalyst was modeled by embedding a metal dimer center into a graphene lattice, where the metal dimer was coordinated with six nitrogen atoms. The rectangular lattice parameter of graphene was 17.22 $\mathring{A} \times$ 17.04 \mathring{A} and the geometric configuration is presented in Fig. 1a.

The free energy change of each ORR elementary step (ΔG) was calculated based on the computational hydrogen electrode (CHE) model proposed by Nørskov and co-workers. 38,39 In this model, the chemical potential of a proton/electron $(H^+ + e^-)$ pair is equal to half that of the gas-phase H2 under standard hydrogen electrode (SHE) conditions. According to the CHE model, ΔG can be defined using eqn (1):

$$\Delta G = \Delta E + \Delta Z P E - T \Delta S + \Delta G_{pH} + \Delta G_{U}$$
 (1)

where ΔE is the total energy change directly obtained from DFT calculations. Δ ZPE and Δ S are the difference of zero-point energy and entropy, respectively. T is the temperature of 298.15 K. $\Delta G_{\rm pH}$ and $\Delta G_{\rm U}$ are caused by variations of the H⁺ concentration and the electrode potential, respectively. Here the value of $\Delta G_{\rm pH}$ is set as zero under acidic conditions. For the free H₂ and H₂O molecules, the entropies were obtained from the NIST database. $S_{\rm H_2}^0$ and $S_{\rm H_2O}^0$ were the entropy under standard conditions obtained from the NIST database $(S_{\rm H_2}^0 = 130.68 \text{ J mol}^{-1} \text{ K}^{-1} \text{ and } S_{\rm H_2O}^0 = 188.84 \text{ J mol}^{-1} \text{ K}^{-1}).$ Then, the calculated entropic term (TS) in the Gibbs free energy at 298.15 K was 0.40 eV for H2 and 0.58 eV for H2O, respectively. 40,41 Note that it is usually difficult to calculate the liquidphase free energies with standard DFT methods. So we applied a correction to our DFT-computed gas phase free energies. This correction is based on the free energy difference between formations of liquid and gas phase H2O from NIST database, and we used a correction of -0.09 eV for H_2O . Thus, the final entropic term of liquid water was 0.67 eV (0.58 + 0.09 = 0.67 eV). For the adsorbates, only vibrational entropy was taken into account to calculate the entropy corrections in the Gibbs free energy due to the negligible contributions of the translational and rotational entropies. The zero-point energies of the free molecules as well as the oxygenated intermediates were calculated from the DFT calculated vibrational frequencies. Specifically, the vibrational frequencies of adsorbed species were calculated by fixing the catalyst substrate. Owing to the highspin ground state of the O2 molecule, they cannot be accurately described in DFT computations.42,43 Thus we calculated all free energies relative to $H_2O(1)$ and $H_2(g)$.

Results and discussion

Catalytic activity of homonuclear BACs

In this work, all 3d, 4d, and 5d transition metals were selected to construct BACs, except for Tc, Cd, and Hg with toxic/

radioactive nature. Thus, 26 metal atoms were considered to construct BACs (Fig. 1b). We will first focus on the activity of homonuclear BACs and then explore more complicated heteronuclear BACs. As revealed by Zelenay and coworkers,44 FeN4 as a catalytically active site for the ORR was directly visualized by aberration-corrected scanning transmission electron microscopy. Amazingly, a high ORR activity can be achieved, when the FeN₄ site was spontaneously ligated by *OH in the fuel cell environment. In addition, some other studies also indicated that *OH species will boost ORR activity and binds on active sites strongly. 45-48 Based on this, a pre-adsorbed OH* species at the metal center was adopted as our BAC model to explore the ORR performance (Fig. 1c). According to previous studies, the oxygen molecule prefers to adsorb onto BACs via a cis-bridged model, which plays an important role in the activation and weakening of O-O bonds, precluding the possibility of the formation of a H2O2 intermediate.26 Therefore, we only considered the 4e⁻ mechanism to form H₂O. Typically, both associative and dissociative mechanisms are considered, depending on whether the O2 molecule dissociates before reduction (detailed pathway seen in SR1-SR4 and SR5-SR9 in the ESI \dagger). Theoretically, the limiting potential (U_L) where all steps are downhill in free energy is usually used as a measure to evaluate the intrinsic activity and the corresponding $U_{\rm L}$ on Pt(111) ($U_{\rm L}=0.80$ V) was set as a benchmark for comparison. Accordingly, M_2/NC with a comparable or more positive U_L value compared to Pt(111) is considered a promising ORR catalyst. In general, the direct O-O cleavage is unfavorable owing to the highly stable and strong O=O bond, and thus we first investigated the associative mechanism. The adsorption free energy of oxygenated intermediates involved in the associative mechanism and the corresponding limiting potential are summarized in Table S1.† In addition, we also investigated the O2 dissociation mechanism. It is found that O2 bonds strongly with early transition metal BACs (including Sc, Ti, V, Cr, Y, Zr, Nb, Mo, Ru, Hf, Ta, W and Re) and can dissociate into two separate O atoms; while for the late transition metal BACs, the O₂ dissociation is energetically very endothermic. Thus, we studied the dissociative mechanism on the abovementioned early transition metal BACs. The adsorption free energy of oxygenated intermediates involved in the dissociative mechanism and the corresponding limiting potential are summarized in Table S2.† The final $U_{\rm L}$ of these early transition metal BACs would adopt a more positive U_L with higher activity between the associative and dissociative mechanism. Fig. 2a presents the $U_{\rm L}$ for the 26 homonuclear M₂/NC BACs. One can clearly see that only Co2/NC can co-balance the adsorption of different reaction intermediates and exhibit outstanding ORR activity comparable to the Pt(111) surface, with a favorable $U_{\rm L}$ of 0.82 V. Noteworthily, among all the investigated homonuclear BACs, the limiting potential of the elements with d orbitals that are less than half filled is negative, which indicates their poor ORR activities. The poor activities are related to their too strong binding interactions with the ORR intermediates. The variation in adsorption free energy is determined by the electronic structure of the active center. As presented in Fig. S1,† with the increasing number of d electrons, the d-band center of the

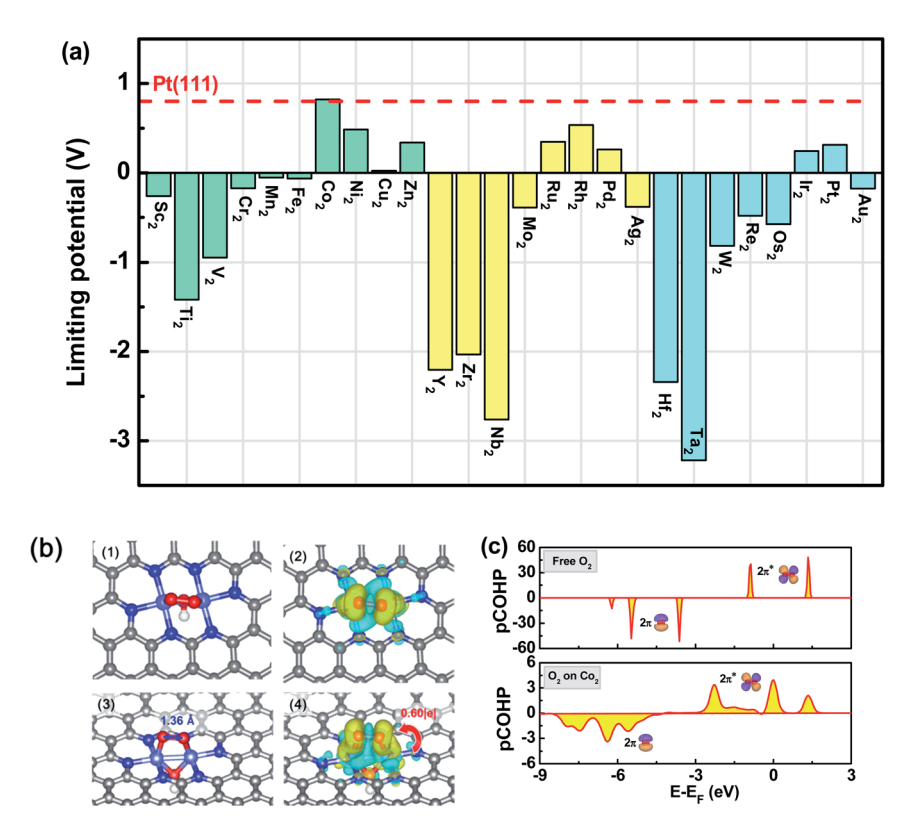


Fig. 2 The ORR activity and electronic characterization of homonuclear BACs. (a) Theoretical limiting potential (U_L) of the 26 homonuclear M₂/NC BACs. (b) Optimized adsorption configuration and charge density difference of O₂ on the Co₂/NC surface. (c) Projected crystal orbital Hamilton population (pCOHP) of free O₂ and O₂ adsorbed on the Co₂/NC surface.

metal dimer tends to become more negative. The higher (the lower) in energy the d band is relative to the highest occupied state (the Fermi energy), the stronger (the weaker) the interaction with the adsorbates. Therefore, a metal dimer with too few or too many d electrons is not suitable for an effective ORR catalyst.

Why does Co₂/NC have a high activity towards the ORR? To address this question, we carefully examined the adsorption and activation of O₂, a key step for the ORR. Our computations demonstrated that O2 is chemisorbed on Co2/NC with a strong adsorption energy of -2.15 eV. As shown in Fig. 2b, O_2 prefers to adsorb by coordination to two Co centers via a cis-bridge configuration. Analyzing the charge density difference revealed that the adsorbed O₂ interacts with Co₂/NC by the socalled "push-pull" mechanism, in which Co2/NC would "push" electrons from the occupied d orbitals into the $2\pi^*$ orbitals of O2, and simultaneously "pull" the lone-pair electrons from the O2 into the unoccupied d orbitals (Fig. 2b). In this case, O2 can be effectively activated with a remarkable O-O bond elongation to 1.36 Å from a gas phase value of 1.24 Å. Bader charge analysis indicated that about 0.60 electrons are transferred from Co_2/NC to O_2 . As a result, the $2\pi^*$ orbitals of O_2 shift down in energy and become broadened and split as compared to the free O₂ molecule, as evidenced by the projected crystal orbital Hamilton population (pCOHP) analysis (Fig. 2c).⁴⁹ The effective activation and weakening of the O-O bond are expected to facilitate the subsequent ORR steps, as confirmed by

the calculated reaction free energies for each ORR elementary step based on the Co_2/NC catalyst (Fig. S2†). At an equilibrium potential of $U=1.23\,\text{V}$ (pink line), the reduction of *O₂ to *OOH (the first reduction step) is the rate-determining step, with an uphill free energy of 0.41 eV. At a thermodynamic limiting potential (blue line) of 0.82 V, all the reaction steps are downhill in free energy. As far as the geometries of the adsorbed intermediates (*OOH, *O and *OH) are concerned, the *O and *OH are co-adsorbed by the two Co–Co atoms, while *OOH is only bonded to one of the Co atoms (for details, see Table S3†).

Catalytic activity of heteronuclear BACs

On the other hand, for most of the studied homonuclear BACs, a volcano-shaped relationship exists between the limiting potential and the adsorption free energy of *OH species ($\Delta G_{^*\mathrm{OH}}$) (Fig. 3a). One can see that $\mathrm{Co_2/NC}$, which exhibits the highest ORR activity among all the studied homonuclear candidates, is located close to the top of the volcano curve. Note that catalysts located on the left side have strong *OH binding strength, and the activities are mainly limited by the step of *OH reduction to $\mathrm{H_2O}$ (*OH + H⁺ + e⁻ \leftrightarrow * + H₂O), and in comparison, those located on the right side exhibit weaker *OH binding, and the ORR activities are limited by the step of *O₂ reduction to *OOH (*O₂ + H⁺ + e⁻ \leftrightarrow *OOH). In principle, a viable ORR catalyst should have moderate adsorption to balance the binding for multiple ORR intermediates, and the limiting potential has to be as positive as possible to drive the occurrence of the reaction.

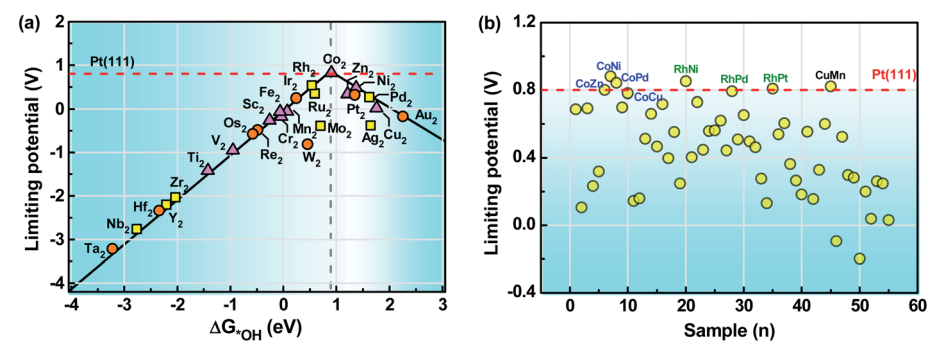


Fig. 3 U_1 of the homonuclear and heteronuclear BACs. (a) Volcano plot relationship between U_1 and the adsorption free energy of *OH based on the homonuclear BACs. (b) The predicted U_L of the 55 heteronuclear BACs; only the promising candidates with comparable activity to the Pt(111) benchmark were shown with compositions.

From Fig. 3a, about 11 homonuclear BACs are identified to be located around the top region of the volcano plot with limiting potential close to or above 0 V, including Fe, Mn, Ir, Ru, Rh, Co, Zn, Ni, Pt, Pd and Cu. Unfortunately, most of them (except for Co) are catalytically unsatisfactory due to the very low limiting potentials. This leaves large room for activity tuning and improvement. Introducing heteronuclear centers by combining two different functional metal sites from either the left branch or right branch of the volcano plot would provide wider tunability and flexibility in modulating the adsorption strengths and ORR activities. Based on this hypothesis, we then extended our study to 55 heteronuclear BACs (M₁M₂/NC) by mixing the above screened 11 metal atoms with $U_{\rm L}$ close to or above 0 V.

Fig. 3b summarizes the calculated $U_{\rm L}$ of the 55 heteronuclear BACs (the detailed adsorption strengths of ORR intermediates for each system are given in Table S4†). Excitingly, 8 of the 55 heteronuclear BACs stand out as highly promising candidates with activity comparable to that of the Pt(111) surface, including four Co-based BACs (CoZn/NC (0.80 V), CoNi/NC (0.88 V), CoPd/NC (0.84 V), and CoCu/NC (0.78 V)), three Rh-based BACs (RhNi/ NC (0.85 V), RhPd/NC (0.79 V), and RhPt/NC (0.81 V)), and CuMn/NC (0.82 V). We should note that 3 heteronuclear BACs (CoNi, CoPd, and RhNi) display more positive U_L values than the homonuclear Co₂/NC counterpart (0.82 V), thus implying the intrinsically higher ORR activity. The optimal adsorption geometries of *OOH, *O, and *OH on the 8 identified BAC systems are depicted in Table S3.† The *O species is usually co-adsorbed and bonded to the two metals. Due to the structural asymmetry of the heteronuclear sites, the adsorption of *OOH and *OH species becomes more complicated. Specifically, for the Co-based CoZn/ NC, CoNi/NC and CoCu/NC systems, the active site to bind the *OOH and *OH intermediates occurs solely at the Co site. While for CoPd/NC, although *OOH and *OH prefer to be co-adsorbed by both the Co and Pd atoms, the intermediates are found to be located much closer to the Co center. Similarly, for the Rh-based BACs, except for RhNi/NC where *OOH is solely bonded to the Rh site, *OH and *OOH prefer to be co-adsorbed by the Rh-Ni, Rh-Pd and Rh-Pt centers, but are geometrically located closer to the Rh site. These results indicate that the introduction of the secondary metals can effectively tune the adsorption of ORR intermediates, yet the main active site for binding *OOH or *OH

species still occurs at the Co or Rh site, which belongs to the same VIII group with nine outer electrons. In fact, if we take a closer look at the activities of the formerly investigated homonuclear BACs (Fig. 2a), it can be observed that from groups 7 to 12 (such as Mn to Zn), with the increasing number of outer electrons, the limiting potential tends to first increase and then decrease. The increased valence electrons in the d-orbitals of the active metal site would partially occupy the M-O antibonding orbital, leading to the weakened adsorption of intermediates. Among them, Co or Rh is just at the right place, which can cobalance the adsorption strength of different intermediates and result in exceptional ORR activity. On the other hand, for the case of the CuMn/NC catalyst, where Cu and Mn are located around two sides of Co, which also facilitates the ORR, the active site for *OOH and *OH binding occurs solely at the Mn site (Table S3†).

Then, we studied the free energy diagrams for O₂ reduction to H₂O on the eight heteronuclear BACs (Fig. S3†). At the equilibrium potential (1.23 V), the activities of the identified CoZn/NC, CoPd/NC, RhNi/NC, RhPt/NC and CuMn/NC candidates are determined by the reduction of *OH to H_2O (*OH + H^+ $+ e^- \leftrightarrow * + H_2O$), whereas those of the CoCu/NC and RhPd/NC catalysts are determined by the reduction from *O2 to *OOH $(*O_2 + H^+ + e^- \leftrightarrow *OOH)$. A particular case is found for the CoNi/NC catalyst, where the activity is determined by two reduction steps (from *O2 to *OOH and from *OH to H2O) having the same value of free energy increase (0.35 eV).

In brief summary, our above analyses screened out one homonuclear and eight heteronuclear BACs with theoretical limiting potentials (between 0.78 V and 0.88 V) comparable and even superior to those of Pt-based materials (~0.80 V), especially the most active BAC, namely CoNi/NC, with a limiting potential of 0.88 V.

In addition to the high activity, stability is another key criterion to evaluate in an electrocatalyst, and only those catalysts with high structural stability can have great potential for synthesis. Thus, we evaluated the stabilities of the above screened BACs by calculating the formation energy (E_f) , which is defined as $E_f = E(MM'@SUB) - E(SUB) - E(M) - E(M')$, where E(MM'@SUB) and E(SUB) are the total energies of BACs and the substrate; E(M) and E(M') denote the total energies of the single metal atom in the bulk phase. According to this definition,

when $E_{\rm f}$ is negative, the formation of bi-atom metal moieties is energetically favorable. As seen in Fig. 4, the E_f values of all our screened BACs have negative formation energies, indicating that the aggregation of metal atoms could be suppressed in thermodynamics. Furthermore, the stability of the substrate has been evaluated using formation energy $(E_f^{'})$ with reference to graphene and nitrogen $(E_{\rm f}^{'}=E({
m SUB})-n\mu_{
m C}-m\mu_{
m N})$, where $E({
m SUB})$ represents the total energy of the substrate, n and m denote the total number of C and N atoms, and $\mu_{\rm C}$ and $\mu_{\rm N}$ are the chemical potentials of C and N atoms, respectively. $\mu_{\rm C}$ and $\mu_{\rm N}$ are calculated from pristine graphene and nitrogen in the gas phase. The $E_{\mathrm{f}}^{'}$ of the substrate used in this work (pyriN6 in Table S5†) is 3.99 eV, which is lower than that of a pyrroN3 substrate (Table S5†). Noteworthily, pyrroN3 has been successfully fabricated and characterized in an experiment. 50 Finally, the $E_{\rm f}^{'}$ of the nine promising BACs was also investigated with reference to graphene and $(E'_{\rm f} = E(MM' \otimes SUB) - n\mu_{\rm C} - m\mu_{\rm N} - E(M) - E(M')).$ From Table S6,† the $E_{\rm f}^{\prime}$ of the nine BACs (2.2–3.3 eV) becomes lower compared with that of the substrate (3.99 eV), indicating that the nine dimers incorporated into the substrate will help to stabilize the system. These results indicated that our screened high-performance homonuclear and heteronuclear BACs exhibit high thermodynamic stabilities and hold strong potential for experimental realizations.

It is worth noting that among the predicted bi-atomic pairs, two heteronuclear (CoNi/NC and CoZn/NC) and one homonuclear (CoCo/NC) BACs have been successfully synthesized by recent experiments, ²³⁻²⁵ and they all demonstrated remarkable ORR performances. In the case of the CoZn/NC electrocatalyst, the *in situ* XANES analysis in the experiment also suggests Co as the major active center during the ORR, ²⁵ which is in good agreement with our theoretical predictions. These experimental results strongly evidenced the predictive power of our computational investigation. With high stabilities and similar inherent ORR potentials, we strongly believe that the other yet unexplored BACs, such as CoCu, CoPd, RhPd, RhPt, RhNi and CuMn, can be realized experimentally in the very near future.

Origin of activity

It is generally accepted that the ORR activity is mainly determined by the adsorption free energy of *OOH, *O and *OH

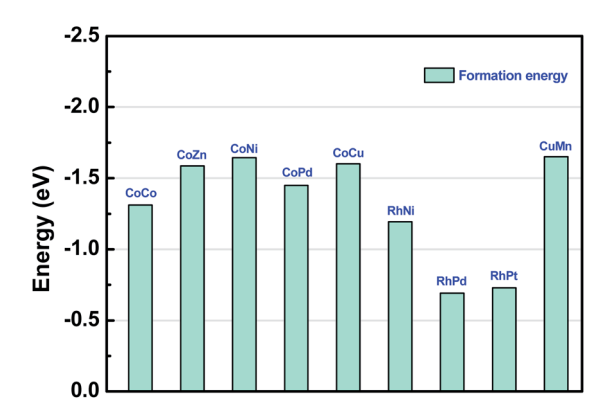


Fig. 4 Formation energy of the nine promising BACs.

species. They tend to scale linearly with each other, leading to the formation of volcano-shaped activity, which is widely applied as a simple descriptor to describe the catalytic activity. 4,51-53 The linear relationships between ΔG_{*OOH} vs. ΔG_{*OH} and ΔG_{*O} vs. ΔG_{*OH} are strongly correlated on traditional transition metal surfaces.53 However, in the case of the studied bi-atom catalysts, we found that their linear relationships are significantly weakened (Fig. 5a and b). This phenomenon can be understood from the significant difference between the intermediate adsorption over BACs and transition-metal surfaces. On the transition-metal surfaces, *OOH (or *OH) prefers to adsorb to the top sites, and *O normally adsorbs on the hollow sites. However for BACs, there are no hollow sites available for *O adsorption, and O* tends to be shared by the two metal centers. Moreover, for *OOH or *OH species, some of them prefer the bridge sites between two metal sites, while others prefer to bind only with one of the metal centers (as seen in Table S3†), showing strong dependence on the heteronuclear bi-atom compositions. Due to these differences, BAC systems are much more complicated than a transition metal surface. Consequently, it is very difficult to precisely describe the ORR activity of BACs with only one descriptor.

Thus, we employed the machine-learning method to explore the correlation between $U_{\rm L}$ and the intrinsic descriptor of the 11 homonuclear and 55 heteronuclear BAC. The success of the machine-learning algorithm depends on the quality of the numerical descriptions of the studied systems. In our case, a feature set with seven descriptors was selected to describe the geometrical and electronic features of BACs, including the distance of two metal atoms (M-M), the average distance between two metal atoms and the coordinated N atoms (M-N), the radii of two metal atoms (R₁ and R₂), the outer electron number of two metal atoms (Ne1 and Ne2), the Pauling electronegativity (P1 and P2), the first ionization energy (I1 and I2) and the electron affinity $(A_1 \text{ and } A_2)$ of the two metals. Note that each heteronuclear dimer corresponds to two sets of BAC compositions (M_1M_2/NC) and $M_2M_1/NC)$, which actually denote the same BACs. Thus, we carried out data enhancement for all the studied heteronuclear BACs, and in this way, each heteronuclear BAC has two sets of input features (Table S7†).

We applied a random forest regressor using a scikit-learn toolkit,54,55 a family of machine learning algorithms, to explore the correlation between the DFT-obtained limiting potential and the feature properties. The input data of U_L obtained from DFT calculations (Tables S1 and S4†) were randomly shuffled and divided into the training set and test set with a ratio of 5:1. As clearly shown in Fig. 5c, our studied model was trained effectively using the random forest regressor with a train score of 0.98 and a test score of 0.90 for the Pearson correlation coefficient. Moreover, a lower mean square error for the training set and test set of 0.004 and 0.022 was achieved, respectively. Furthermore, the importance of the selected seven features, which are closely related to the geometric and chemical properties affecting the catalytic performance, was also evaluated (Fig. 5d). The features of M-N and M-M distances are found to be the paramount factors affecting the ORR activity of BACs with a feature importance of 0.41 and 0.25, respectively. In

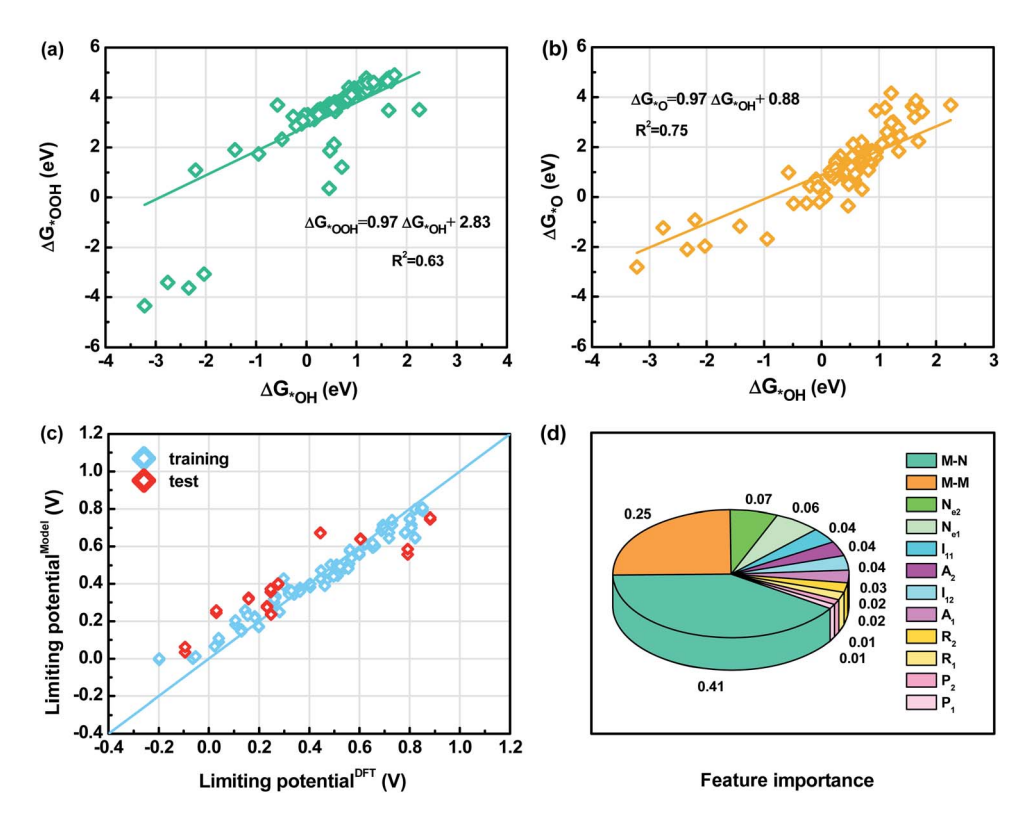


Fig. 5 Linear relationships among the adsorption free energy obtained from DFT calculations (a and b) and results of machine-learning (c and d). (a and b) Linear relationships of ΔG_{*OOH} vs. ΔG_{*OH} and ΔG_{*O} vs. ΔG_{*OH} on heteronuclear BACs. (c) Comparison of DFT-obtained U_L with predicted values. (d) The feature importance based on a random forest regressor.

particular, the delicate activity difference in the Co-based and Rh-based heteronuclear BACs can be rationalized to be a result of the geometry difference induced by the secondary metal. We should note that the outer electron number of metal atoms (Ne) also plays an important role, although the influence becomes less prominent (with a feature importance of 0.13). This can be understood by the formation of a metal-metal bond between two metal atoms and these electrons cannot significantly help in binding ORR intermediates. Specifically, the Co center and Rh center with suitable outer electrons tend to exhibit a high activity, while the other four descriptors have a relatively low feature importance. In addition, the M-M distance in homonuclear BACs and the corresponding values in bulk metals have been summarized in Table S8.† One can see that among the investigated homonuclear BACs, the M-M distance is shorter than that in the bulk phase except for Co. This helps to explain and understand the difference in the ORR performance of BACs, and the machine-learning method is a powerful tool to establish the intrinsic structure-property correlation.

Conclusion

BACs have recently emerged as a new frontier in electrocatalysis. In this work, we explored the potential of atomically dispersed bi-atom catalysts (BACs) for the ORR by means of systematic and comprehensive DFT computations coupled with machine-learning techniques. We first sampled

homonuclear (M₂/NC) BACs covering 26 transition metal atoms, and then constructed 55 heteronuclear BACs based on the activity volcano curve of the homonuclear catalysts. Our screening process identified that one homonuclear (Co2/NC) BAC and eight heteronuclear BACs (CoZn/NC, CoNi/NC, CoPd/ NC, CoCu/NC, RhNi/NC, RhPd/NC, RhPt/NC, and CuMn/NC) are highly promising alternatives to Pt-based catalysts. Among them, CoNi/NC possesses the most optimal activity with a very high limiting potential of 0.88 V. Furthermore, aided by the machine-learning method, we revealed the key factors that govern the ORR activity of BACs. The results indicated that the ORR activity of BACs is mainly governed by simple geometric parameters (e.g., the distance of two metal atoms as well as the average distance between two metal atoms and the coordinated N atoms) and the physical properties of the metal atoms (e.g., outer electron number). Motivated by the recent experimental progress in fabricating BACs, we conclude that our identified promising BACs hold great potential for future synthesis in experiments. This work not only identifies highly promising BACs to replace precious Pt catalysts but also provides useful insights for the design of high-performance electrocatalysts for the ORR and other related electrochemical reactions.

Conflicts of interest

The authors declare no competing financial interests.

Acknowledgements

This work was supported in China by the Science and Technology Research Program of Chongqing Municipal Education Commission (Grant No. KJQN201801608), the Program of Innovation Center for Lipid Resource Utilization at Chongging University of Education (No. 2017XJPT01), the Program for Innovative Research Team in Chongging University of Education (No. CQYC201903178), the National Natural Science Foundation of China (No. 21903008), the Chongqing Municipal Resources and Society Security Bureau (cx2019141), the Science Technology Chongqing and Commission (cstc2020jcyjmsxmX0382), and the Fundamental Research Funds for the Central Universities (2020CDJQY-A031 and 2020CDJ-LHZZ-063), and in the USA by the NSF Center for the Advancement of Wearable Technologies (Grant 1849243). This research used resources of the National Supercomputer Center in Guangzhou.

References

- 1 B. C. H. Steele and A. Heinzel, *Nature*, 2001, **414**(6861), 345–352.
- 2 M. Winter and R. J. Brodd, Chem. Rev., 2004, 104(10), 4245–4270.
- 3 A. A. Gewirth, J. A. Varnell and A. M. DiAscro, *Chem. Rev.*, 2018, **118**(5), 2313–2339.
- 4 A. Kulkarni, S. Siahrostami, A. Patel and J. K. Nørskov, *Chem. Rev.*, 2018, **118**(5), 2302–2312.
- 5 P. C. K. Vesborg and T. F. Jaramillo, *RSC Adv.*, 2012, 2(21), 7933–7947.
- 6 Y. Wang, Y. Li and T. Heine, *J. Am. Chem. Soc.*, 2018, **140**(40), 12732–12735.
- 7 Z. Lu, G. Xu, C. He, T. Wang, L. Yang, Z. Yang and D. Ma, Carbon, 2015, 84, 500-508.
- 8 C. Deng, F. Li and Q. Tang, J. Phys. Chem. C, 2019, 123(44), 27116–27123.
- 9 L.-y. Feng, Y.-j. Liu and J.-x. Zhao, J. Power Sources, 2015, 287, 431–438.
- 10 Y. Wang, Y.-J. Tang and K. Zhou, *J. Am. Chem. Soc.*, 2019, **141**(36), 14115–14119.
- 11 V. R. Stamenkovic, B. S. Mun, M. Arenz, K. J. J. Mayrhofer, C. A. Lucas, G. Wang, P. N. Ross and N. M. Markovic, *Nat. Mater.*, 2007, **6**, 241–247.
- 12 C. Wang, N. M. Markovic and V. R. Stamenkovic, *ACS Catal.*, 2012, 2(5), 891–898.
- 13 Z. Duan and G. Wang, *Phys. Chem. Chem. Phys.*, 2011, **13**(45), 20178–20187.
- 14 H. A. Hansen, J. Rossmeisl and J. K. Nørskov, *Phys. Chem. Chem. Phys.*, 2008, **10**(25), 3722–3730.
- 15 H. Zhang, G. Liu, L. Shi and J. Ye, *Adv. Energy Mater.*, 2018, **8**(1), 1701341.
- 16 X.-F. Yang, A. Wang, B. Qiao, J. Li, J. Liu and T. Zhang, *Acc. Chem. Res.*, 2013, **46**(8), 1740–1748.
- 17 Y. Wang, J. Mao, X. Meng, L. Yu, D. Deng and X. Bao, *Chem. Rev.*, 2019, **119**(3), 1806–1854.

- 18 S. Ding, M. J. Hulsey, J. Perez-Ramirez and N. Yang, *Joule*, 2019, 3(12), 2897–2929.
- 19 Y. Pan, C. Zhang, Z. Liu, C. Chen and Y. Li, *Matter*, 2020, 2(1), 78–110.
- 20 Z. Li, S. Ji, Y. Liu, X. Cao, S. Tian, Y. Chen, Z. Niu and Y. Li, *Chem. Rev.*, 2020, **120**(2), 623–682.
- 21 C. Wan, X. Duan and Y. Huang, *Adv. Energy Mater.*, 2020, **10**(14), 1903815.
- 22 J. Wang, W. Liu, G. Luo, Z. Li, C. Zhao, H. Zhang, M. Zhu, Q. Xu, X. Wang, C. Zhao, Y. Qu, Z. Yang, T. Yao, Y. Li, Y. Lin, Y. Wu and Y. Li, *Energy Environ. Sci.*, 2018, 11(12), 3375–3379.
- 23 M. Xiao, H. Zhang, Y. Chen, J. Zhu, L. Gao, Z. Jin, J. Ge, Z. Jiang, S. Chen, C. Liu and W. Xing, *Nano Energy*, 2018, 46, 396–403.
- 24 X. Han, X. Ling, D. Yu, D. Xie, L. Li, S. Peng, C. Zhong, N. Zhao, Y. Deng and W. Hu, Adv. Mater., 2019, 31(49), 1905622.
- 25 Z. Lu, B. Wang, Y. Hu, W. Liu, Y. Zhao, R. Yang, Z. Li, J. Luo, B. Chi, Z. Jiang, M. Li, S. Mu, S. Liao, J. Zhang and X. Sun, *Angew. Chem.*, 2019, 131(9), 2648–2652.
- 26 M. Xiao, Y. Chen, J. Zhu, H. Zhang, X. Zhao, L. Gao, X. Wang, J. Zhao, J. Ge, Z. Jiang, S. Chen, C. Liu and W. Xing, *J. Am. Chem. Soc.*, 2019, 141(44), 17763–17770.
- 27 X. Y. Guo, J. X. Gu, S. R. Lin, S. L. Zhang, Z. F. Chen and S. P. Huang, *J. Am. Chem. Soc.*, 2020, **142**(12), 5709–5721.
- 28 F. Li, X. Liu and Z. Chen, Small Methods, 2019, 3, 1800480.
- 29 J. Zhao, J. Zhao, F. Li and Z. Chen, *J. Phys. Chem. C*, 2018, **122**(34), 19712–19721.
- 30 F. Li and Z. Chen, Nanoscale, 2018, 10(33), 15696-15705.
- 31 G. Kresse and J. Furthmüller, *Phys. Rev. B: Condens. Matter Mater. Phys.*, 1996, 54(16), 11169–11186.
- 32 J. P. Perdew, K. Burke and M. Ernzerhof, *Phys. Rev. Lett.*, 1996, 77(18), 3865–3868.
- 33 P. E. Blöchl, Phys. Rev. B: Condens. Matter Mater. Phys., 1994, 50(24), 17953–17979.
- 34 S. Grimme, J. Antony, S. Ehrlich and H. Krieg, *J. Chem. Phys.*, 2010, **132**(15), 19.
- 35 M. Fishman, H. L. L. Zhuang, K. Mathew, W. Dirschka and R. G. Hennig, *Phys. Rev. B: Condens. Matter Mater. Phys.*, 2013, **87**(24), 245402.
- 36 K. Mathew, R. Sundararaman, K. Letchworth-Weaver, T. A. Arias and R. G. Hennig, *J. Chem. Phys.*, 2014, **140**(8), 084106.
- 37 H. Johll, H. C. Kang and E. S. Tok, *Phys. Rev. B: Condens. Matter Mater. Phys.*, 2009, **79**(24), 18.
- 38 J. K. Nørskov, J. Rossmeisl, A. Logadottir, L. Lindqvist, J. R. Kitchin, T. Bligaard and H. Jónsson, *J. Phys. Chem. B*, 2004, **108**(46), 17886–17892.
- 39 J. Rossmeisl, A. Logadottir and J. K. Norskov, *Chem. Phys.*, 2005, 319(1-3), 178–184.
- 40 X. Zhang, K. A. Min, W. Zheng, J. Hwang, B. Han and L. Y. S. Lee, *Appl. Catal.*, *B*, 2020, 273, 118927.
- 41 K. Nam, H. Chun, J. Hwang, K.-A. Min and B. Han, ACS Sustainable Chem. Eng., 2020, 8(29), 10852–10858.
- 42 R. O. Jones and O. Gunnarsson, *Rev. Mod. Phys.*, 1989, **61**(3), 689–746.

- 43 S. Kurth, J. P. Perdew and P. Blaha, Int. J. Quantum Chem., 1999, 75(4-5), 889-909.
- 44 H. T. Chung, D. A. Cullen, D. Higgins, B. T. Sneed, E. F. Holby, K. L. More and P. Zelenay, Science, 2017, 357(6350), 479-483.
- 45 A. Zitolo, V. Goellner, V. Armel, M.-T. Sougrati, T. Mineva, L. Stievano, E. Fonda and F. Jaouen, Nat. Mater., 2015, 14(9), 937-942.
- 46 Y. H. Zhao, J. X. Gu and Z. F. Chen, Adv. Funct. Mater., 2019, 29(44), 1904782.
- 47 E. F. Holby and C. D. Taylor, Sci. Rep., 2015, 5, 9286.
- 48 J. Wang, Z. Q. Huang, W. Liu, C. R. Chang, H. L. Tang, Z. J. Li, W. X. Chen, C. J. Jia, T. Yao, S. Q. Wei, Y. Wu and Y. D. Lie, J. Am. Chem. Soc., 2017, 139(48), 17281-17284.

- 49 S. Maintz, V. L. Deringer, A. L. Tchougreeff and R. Dronskowski, J. Comput. Chem., 2016, 37(11), 1030-1035.
- 50 D. C. Wei, Y. Q. Liu, Y. Wang, H. L. Zhang, L. P. Huang and G. Yu, Nano Lett., 2009, 9(5), 1752-1758.
- 51 N. Govindarajan, M. T. M. Koper, E. J. Meijer and F. Calle-Vallejo, ACS Catal., 2019, 9(5), 4218-4225.
- 52 M. Anand and J. K. Nørskov, ACS Catal., 2020, 10(1), 336-345.
- 53 V. Viswanathan, H. A. Hansen, J. Rossmeisl and J. K. Nørskov, ACS Catal., 2012, 2(8), 1654-1660.
- 54 L. Breiman, *Machine Learning*, 2001, **45**(1), 5–32.
- 55 O. Kramer, Scikit-learn, Machine Learning for Evolution Strategies, Springer, 2016, pp. 45-53.